



## Heterostructured Ti-doped ZnO/Ag metal: an efficient photocatalyst for dye degradation in sunlight

Sandeep Kanade<sup>a</sup>, Dnyaneshwar R. Shinde<sup>a,\*</sup>, K.G. Kanade<sup>a,b</sup>

<sup>a</sup>Pune District Education Association's Prof. Ramkrishna More College (Affiliated to SPPU), Akurdi, Pune 411044, India, Tel. (095)9881350383; emails: drshinde1970@yahoo.com (D.R. Shinde), skanade509@gmail.com (S. Kanade), kgkanade@yahoo.co.in (K.G. Kanade)

<sup>b</sup>Rayat Education Society's Science College (Affiliated to Shivaji University), Satara, India

Received 1 June 2016; Accepted 28 October 2016

### ABSTRACT

Silver metal/Ti-doped ZnO, silver metal/ZnO, Ti(IV)-doped ZnO and ZnO photocatalysts were obtained by thermal decomposition of respective oxalate precursors. The synthesized photocatalysts were characterized by chemical and spectroscopic methods. The doping of ZnO with Ti(IV) and the formation of silver metal heterostructures in ZnO nanostructures were confirmed through powder X-ray diffraction and tunneling electron microscopy analysis. The ZnO and Ti-doped ZnO have crystallized in hexagonal wurtzite structure while heterostructured catalysts showed the presence of additional cubic crystalline phase belonging to Ag metal. Surface morphology was observed through scanning electron microscopic imaging while surface area was determined by Brunauer–Emmett–Teller method. The photocatalytic activity of the photocatalysts was studied on the structurally diverse dyes in the sunlight and under optimized conditions of pH of dye solutions and catalyst dose. The degradation of dyes was measured in terms of decolourization as well as chemical oxygen demand. The photocatalytic activities of the catalysts were compared in terms of first-order rate constants of the decolourization of dyes. The photocatalytic activity of the heterostructured Ag metal/Ti-doped ZnO catalysts was found superior to the photocatalytic activity of ZnO, silver metal/ZnO and Ti-doped ZnO catalysts.

*Keywords:* ZnO; Photocatalyst; Heterostructure; Dye degradation; Sunlight

### 1. Introduction

Dyes are the coloured organic compounds, which are often employed for colouring a wide variety of the consumer products. To meet the requirement of different industries, every year, large quantities of structurally and chemically diverse dyes are manufactured. Consequently, they are released in large quantities into surrounding water bodies thereby emerged as one of the major water pollutants. Effluents released from dye production and textile dyeing industries are the major sources of dyes in the aquatic environment. Approximately 12% of the dyes applied to textiles are lost during processing operations [1]. Many dyes and

their degradation products in water are reported as toxic, carcinogenic, and mutagenic chemical species [2]. Hence, removal of dyes from effluents is biologically and environmentally important. Photocatalytic degradation driven by sunlight is one of the emerging technologies useful for the complete mineralization of a wide range of organic dyes and organic pollutants [3–5]. Nanocrystalline ZnO has proven to be a promising photocatalyst for this purpose owing to its high activity in sunlight, low cost, and environment-friendly nature [2,6,7]. Furthermore, it possesses high quantum efficiency, high redox potential, and high physical and chemical stability as well as advantages such as ease of preparation, and very low toxicity [2,3,6–9]. However, the principal drawbacks of nanocrystalline ZnO are a rapid recombination rate of the photogenerated

\* Corresponding author.

electron–hole pairs and the inefficient utilization of sunlight. These drawbacks hamper the applications of ZnO to utilize it in the large-scale treatment of effluents containing dyes [10–15]. Several strategies such as doping ZnO with metallic or non-metallic ions, coupling ZnO with other semiconductor materials, and sensitizing ZnO with lower band gap materials were adopted to overcome these limitations [16–25]. ZnO–noble metal-type nanoheterostructures are among the most promising hybrid materials that enhance the photocatalytic activity of ZnO [18,26]. In the present study, we have attempted to enhance the photocatalytic activity of ZnO by simultaneously doping it with Ti(IV) and coupling it with nanocrystalline silver metal particles, which represents hybrid catalyst system. Furthermore, the photocatalytic activities of the catalysts were evaluated on three structurally diverse dyes in the presence of sunlight. Finally, from application viewpoint, mineralization of dyes was studied at pilot scale in channel reactor using Ag metal/Ti-doped ZnO as a photocatalyst.

## 2. Materials and methods

### 2.1. Synthesis of photocatalysts

All the chemicals used in the present study are of analytical reagents grade (Loba Chemi Pvt. Ltd., Mumbai, India) and were used without further purification.

ZnO, Ti-doped ZnO, and heterostructured Ti-doped ZnO/Ag metal photocatalysts were prepared by the thermal decomposition of oxalate precursors according to the prescribed method [27]. Zinc oxalate precursor was prepared by the dry chemical reaction between zinc acetate and oxalic acid in mortar. These two reactants were mixed in 1:1.1 molar proportion in an agate mortar and ground until the odour of acetic acid completely disappeared. The precursor was then decomposed to ZnO in an open atmosphere by heating on a Bunsen burner in a platinum crucible followed by annealing at 600°C for 1.5 h in a muffle furnace. Similarly, Ti(IV)-doped ZnO photocatalyst and heterostructured Ti(IV)-doped ZnO/Ag metal photocatalysts were synthesized, wherein calculated quantities of AgNO<sub>3</sub> and Ti(OH)<sub>4</sub> were added to the reaction mixture during the preparation of the precursors. Ti(OH)<sub>4</sub> was obtained by the precipitation of appropriate quantity of TiCl<sub>4</sub> with ammonia followed by centrifugation.

### 2.2. Characterization of photocatalysts

The content of Zn(II), Ag metal, and Ti(IV) in the synthesized photocatalysts were confirmed by chemical analysis using prescribed methods [28]. Furthermore, the elements in synthesized catalysts were confirmed by SEM–EDS analysis. The crystal phase of the photocatalysts was confirmed by powder X-ray diffraction (XRD) analysis, whereas particle morphology was studied through scanning electron microscopic (SEM) and Tunneling electron microscopy (TEM) imaging. The band gap was obtained from diffuse reflectance spectra (DRS) using pure powdered BaSO<sub>4</sub> as reference material. Specific surface areas were measured with Brunauer–Emmett–Teller (BET) method using N<sub>2</sub> gas. Photoluminescence (PL) spectra were recorded at room temperature using an excitation wavelength of 350 nm.

### 2.3. Determination of photocatalytic activity

The photocatalytic activities of catalysts were evaluated on structurally diverse dyes: crystal violet, Orange M2R (OM-2R), and amido black B-10 (ABB) (supplementary file, Table S-1 and Figs. S-1(a–c)) under solar irradiation (intensity:  $5.9 \times 10^3$ – $6.8 \times 10^3$  lx). The reactions were performed under optimized condition of pH (pH = 10 for CV and pH = 11 for OM-2 R and ABB; supplementary file, Figs. S-2(a–c)) and catalyst dose (0.4 g L<sup>-1</sup> of the dye solution) (supplementary file, Table S-2). The solutions of dyes (concentration 10 mg L<sup>-1</sup>) were prepared separately in distilled water, and the pH was adjusted by the addition of NaOH.

In the kinetics of decolourization dyes, 100 mL of the dye solution was sonicated with 30 mg photocatalyst; the resulting suspension was poured into Petri plates (area = 125 cm<sup>2</sup>) and placed in sunlight. At a definite time interval, 5 mL dye solution was withdrawn, and the absorbance was recorded at the  $\lambda_{\max}$  of the dye solution [2,29]. The percentage decolourization was calculated using Eq. (1):

$$\text{Percent decolourization} = \frac{A_0 - A}{A_0} \times 100 \quad (1)$$

where  $A_0$  is the initial absorbance of the dye at  $\lambda_{\max}$ , and  $A$  is the absorbance of the dye solution at  $\lambda_{\max}$  after the experiment. From the experimental data, first-order rate constants were determined by a graphical method [29]. The photocatalytic activities of the photocatalysts were compared in terms of the first-order rate constants.

Finally, photo degradation of the dyes was performed in a channel reactor (tabletop model of area 0.4 m<sup>2</sup> and capacity 4 L; supplementary file, Fig. S-3) of which design and working were explained elsewhere [30]. It was installed in sunlight. Suspensions of the particular photocatalyst were prepared in the dye solution by stirring, and the pH was adjusted to the requisite value and then allowed to pass through a reactor at controlled flow rate (CV = 15 mL/min, ABB and OM-2R = 10 mL/min; these are the optimized flow rates for optimum mineralization of the dyes). In this experiment, decolourization was evaluated by the decrease in absorbance, whereas mineralization in terms of the decrease in chemical oxygen demands (COD) measurement [28]. The recyclability of catalysts was studied by repetitive use of the recovered catalyst.

## 3. Results and discussion

A preliminary study indicated that Ti<sub>0.05</sub>Zn<sub>0.95</sub>O exhibited highest catalytic activity among the various catalysts prepared by doping different levels of Ti(IV) in ZnO. Hence, in next step, we have synthesized heterostructured catalysts containing various percentages of Ag metal in Ti<sub>0.05</sub>Zn<sub>0.95</sub>O. Among the catalysts containing various percentages of Ag metal in Ti<sub>0.05</sub>Zn<sub>0.95</sub>O, the catalyst containing ~7% Ag metal exhibited highest photocatalytic activity (supplementary file, Table S-3). Therefore, herein, we have compared the photocatalytic activities of typical catalysts, which are Ag metal (7%)/Ti<sub>0.05</sub>Zn<sub>0.95</sub>O (Ag/TiZnO), Ag metal (7%)/ZnO (Ag/ZnO), and Ti<sub>0.05</sub>Zn<sub>0.95</sub>O (TiZnO) with pure ZnO (ZnO) [31].

### 3.1. Chemical analysis

Chemical analyses of the photocatalysts were performed for Zn(II), Ti(IV), and Ag metal (Table 1). The observed percentage of the constituents in the synthesized catalysts was concurred with expected stoichiometry of the catalyst. Furthermore, EDS analysis of catalysts (Fig. 1) was performed, which showed the presence of respective elements in requisite proportion in photocatalysts (see also supplementary file, Figs. S-4(a–c)).

### 3.2. XRD characteristics

Fig. 2 shows the powder XRD pattern of the ZnO, Ag/ZnO, TiZnO, and Ag/TiZnO photocatalysts. The diffraction peaks in XRD of all four catalysts at  $2\theta = 31.77^\circ, 34.42^\circ, 36.24^\circ, 47.55^\circ, 56.59^\circ, 62.88^\circ, 66.39^\circ, 67.94^\circ,$  and  $69.09^\circ$  can be indexed to the different planes of hexagonal phase of ZnO (Joint committee on powder diffraction standards (JCPDS) card no. 36-1451) [2]. The diffraction data obtained from these peaks concurred with the JCPDS card for ZnO (calculated crystal characteristics are lattice parameters:  $a = 3.2499 \text{ \AA}$  and  $c = 5.2065 \text{ \AA}$ , X-ray density =  $5.6751 \text{ g/cm}^3$ , crystal volume =  $4.76 \times 10^{-23} \text{ cm}^3$ , and Zn–O bond length =  $1.9785 \text{ \AA}$ ).

The peaks in the XRD of the catalysts Ag/ZnO and Ag/TiZnO can be ascribed as two different sets. The first set of peaks ( $2\theta = 31.77^\circ, 34.42^\circ, 36.24^\circ, 47.55^\circ, 56.59^\circ, 62.88^\circ, 66.39^\circ, 67.94^\circ,$  and  $69.09^\circ$ ) corresponds to the hexagonal phase of ZnO (JCPDS card no. 36-1451) while the second set of peaks ( $2\theta = 38.13^\circ, 44.85^\circ, 64.91^\circ,$  and  $77.85^\circ$ ) can be indexed to face centered cubic (FCC) crystal structure of Ag metal (JCPDS card no. 04-0783) [9,26]. Furthermore, the XRD data obtained from the second set of peaks showed best agreement with JCPDS card of silver metal (calculated crystal characteristics are lattice constant:  $a = 4.0843 \text{ \AA}$ ,

atomic size Ag =  $1.444 \text{ \AA}$ , X-ray density =  $10.4504 \text{ g cm}^{-3}$ , and unit cell volume =  $6.8132 \times 10^{-23} \text{ cm}^3$ ). The XRD patterns of Ag/ZnO and Ag/TiZnO reveal that in these catalysts, ZnO and Ag metal crystallites exist together. Extra peaks are not observed in the XRD TiZnO and Ag/TiZnO other than hexagonal and FCC phases, indicating that the doping of Ti(IV) has taken place perfectly in ZnO to form single crystalline phase. The perfect doping of Ti(IV) in ZnO is due to the comparable ionic sizes Ti(IV) and Zn(II) ions as well as relatively low amount Ti(IV) in the catalysts. The formation of Ag metal particles in the catalysts is a result of the annealing of the catalysts in an oxygen-rich environment above the stability temperature of  $\text{Ag}_2\text{O}$  [8]. Georgekutty et al. [32] reported that  $\text{Ag}_2\text{O}$  is stable up to  $300^\circ\text{C}$ , beyond which it decomposes to form metallic silver (Eq. (2)) [7]:



The crystallite size of the different catalysts was calculated by Debye–Shereer’s formula and was found to be 32 nm for pure ZnO, 28 nm for TiZnO, 29 nm of ZnO, 26 nm for Ag metal in Ag/ZnO, 24 nm for TiZnO, and 18 nm for Ag metal in Ag/TiZnO catalysts.

### 3.3. Morphology and microstructure

The surface morphology of the synthesized photocatalysts was investigated through SEM imaging (Figs. 3(a)–(d)). These images clearly reveal the presence of a large number of bunched nanorod-like structures in ZnO and thin nanosheet-like structures in Ag/ZnO.

Table 1  
Percent content of the metal ions in the photocatalysts

Catalyst	Content (% by weight)		
	Zn(II)	Ag metal	Ti(IV)
ZnO	80.03 ± 0.32	0.00	0.00
TiZnO	72.31 ± 0.18	0.00	6.27 ± 0.49
Ag/ZnO	69.56 ± 0.22	12.06 ± 0.06	00.00
Ag/TiZnO	71.78 ± 0.06	6.74 ± 0.14	2.81 ± 0.32

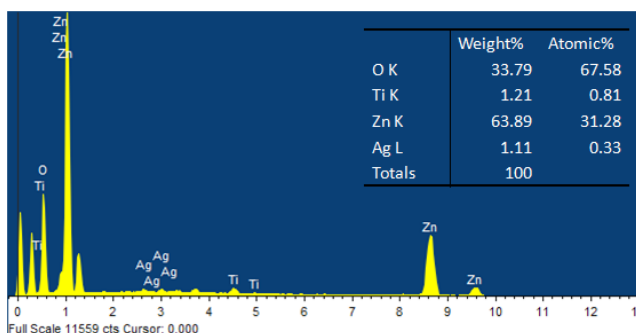


Fig. 1. EDS of Ag metal/TiZnO catalyst.

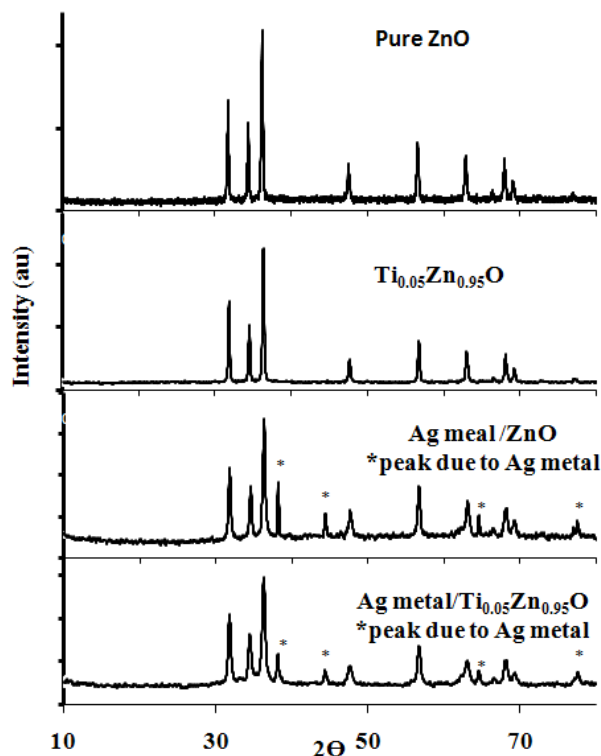


Fig. 2. XRD of photocatalysts.



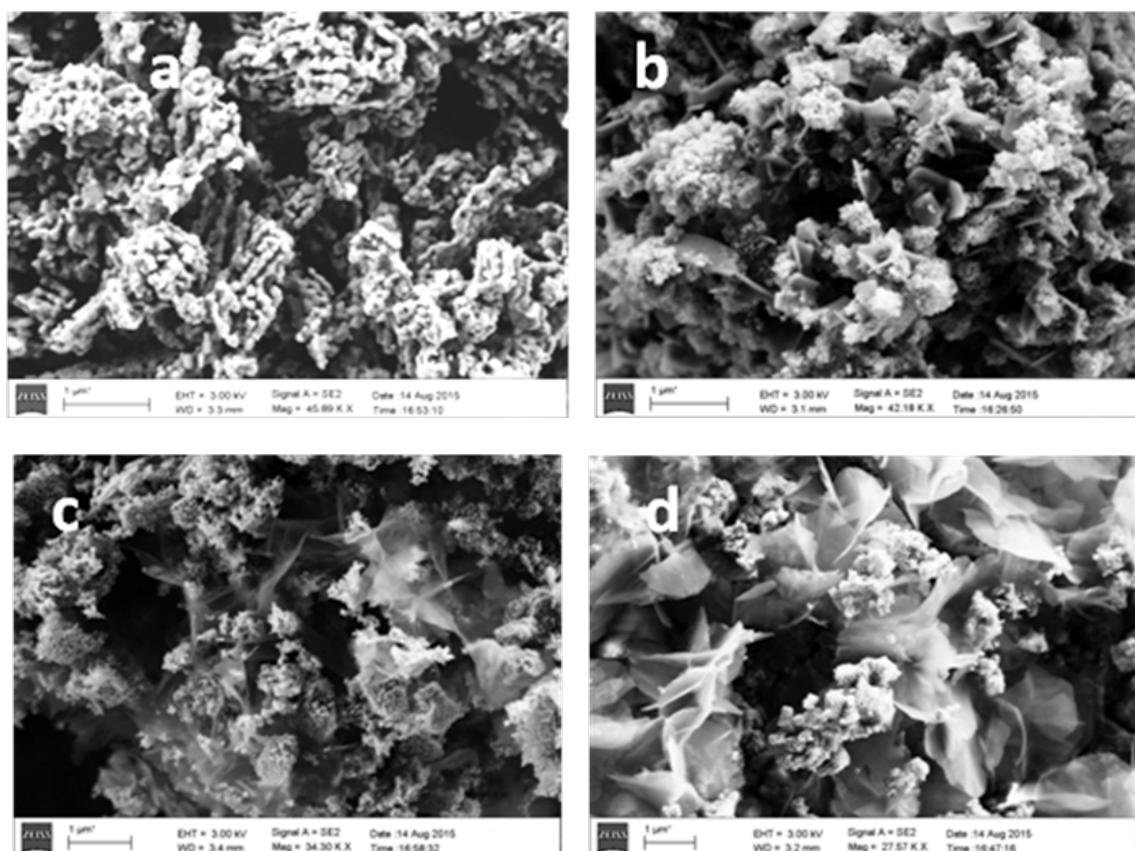


Fig. 3. SEM images of: (a) pure ZnO, (b) TiZnO, (c) Ag/TiZnO, and (d) Ag/ZnO.

In depth, further structural information of the photocatalysts was obtained by TEM imaging (Figs. 4(a)–(d)). From a low magnification TEM image, size and shape of photocatalyst particles were observed. It showed the presence of nanostructured particles (average particle size for ZnO, 64 nm, and for Ag/TiZnO, 37 nm) of anisotropic shapes in the photocatalysts. High resolution tunneling electron microscopy (HRTEM) images of ZnO photocatalyst clearly showed a lattice spacing of 2.8, 2.48, and 1.47 Å belonging to (100), (101), and (103) planes of hexagonal crystal structure. The lattice spacing in Ag/TiZnO photocatalyst was observed at 2.8 and 1.64 Å that belong to (100) and (110) planes of hexagonal crystal structure of ZnO. Furthermore, the lattice spacing of 2.32 Å was observed in Ag/TiZnO that belongs to (111) plane of cubic crystal structure of silver metal. Thus, HRTEM images of Ag/TiZnO photocatalyst indicated the presence of heterostructured silver metal in ZnO. Selected area diffraction pattern shows concentric rings consisting of distinct spots, which suggest the crystalline structure of photocatalysts. The presence of silver metal in heterostructured photocatalysts is also indicated by thin mesh-like structure in TEM image of the photocatalyst (Fig. 4(c)).

#### 3.4. Band gap

Fig. 5 depicts K–M plots of photocatalysts [33] while Fig. 6 represents the diffuse UV-visible spectra in absorbance mode. The band gap was obtained from K–M plot by extrapolation of the linear vertical region to the energy axis, and

they are 3.20 eV for ZnO and TiZnO, 3.16 eV for Ag/TiZnO, and 3.31 eV for Ag/ZnO. This observation indicates that band gap of ZnO is affected by Ti(IV) doping as well by presence of Ag metal nanoparticles in it, and among the presented catalysts, Ag/TiZnO exhibited lowest band gap. The absorption spectrum heterostructured catalysts (Fig. 6) showed strong absorption in visible region indicating enhanced absorption of visible light due to the presence of Ag metal [26].

#### 3.5. Photoluminescence spectroscopic characterization

Typical PL spectra of the synthesized catalysts at excitation wavelength 350 nm are presented in Fig. 7. The PL spectrum of ZnO is composed of two emission bands: one in the UV region and the other in the visible region. Furthermore, the broad emission band in the visible region consists of sharp emission peaks at 407, 439, 458, 475, and 483 nm. The emission band in the UV region can be assigned to a near band-edge emission while the peaks in the visible region can be attributed to the defects in ZnO [34,35]. In the PL spectrum of ZnO, the band-edge emission peak is centred at 384 nm, whereas a small shift in the position of this band to higher wavelength is observed in PL spectra of TiZnO and Ag/TiZnO. The intensity of the bands in the PL spectrum of ZnO is significantly quenched in the spectra of TiZnO, AgZnO, and Ag/TiZnO catalysts, indicating the existence of a direct interaction between Ag metal and ZnO crystallites. The direct interaction between ZnO and Ag metal particles

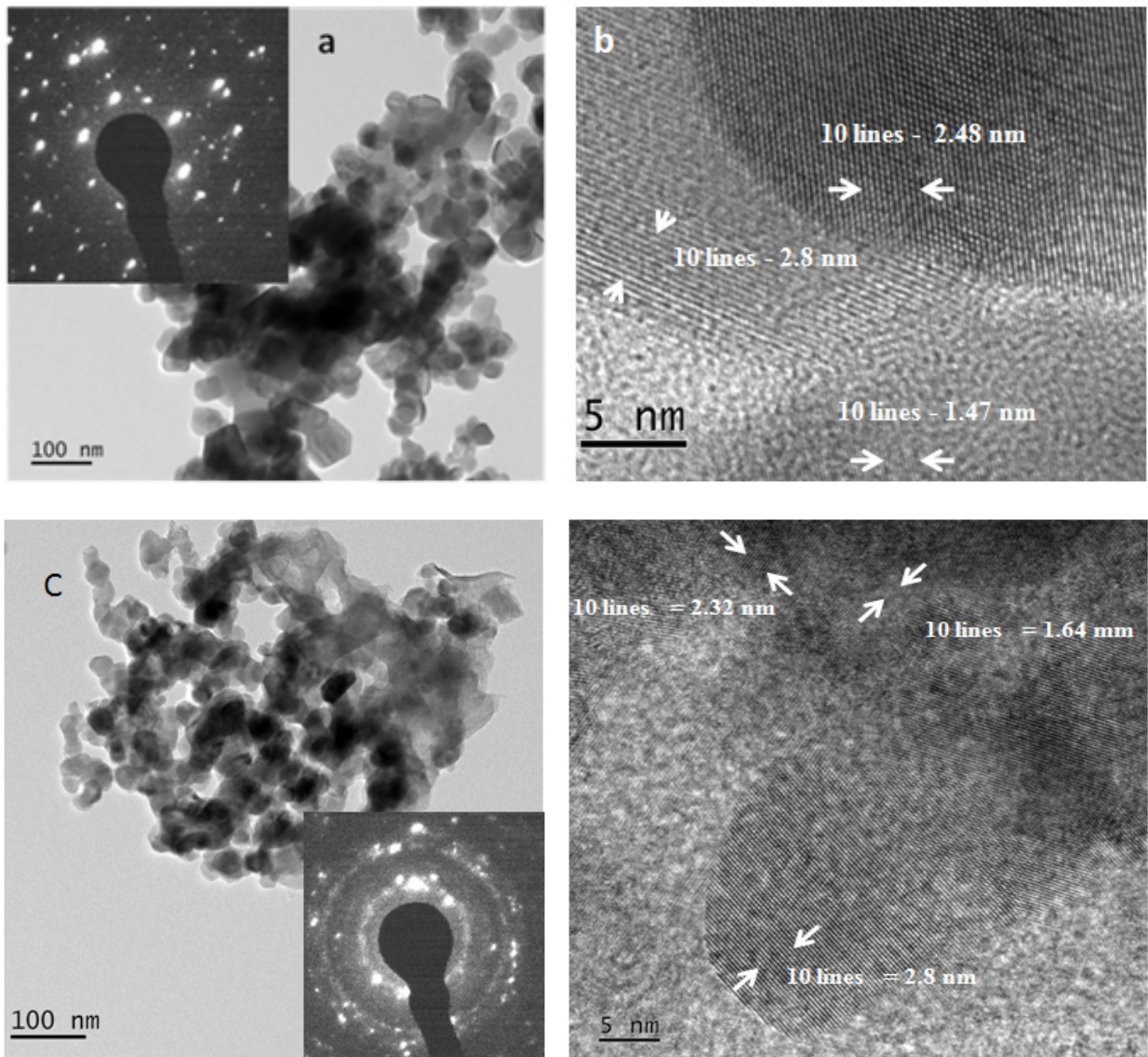


Fig. 4. TEM micrographs of pure ZnO (a and b) and Ag/TiZnO (c and d).

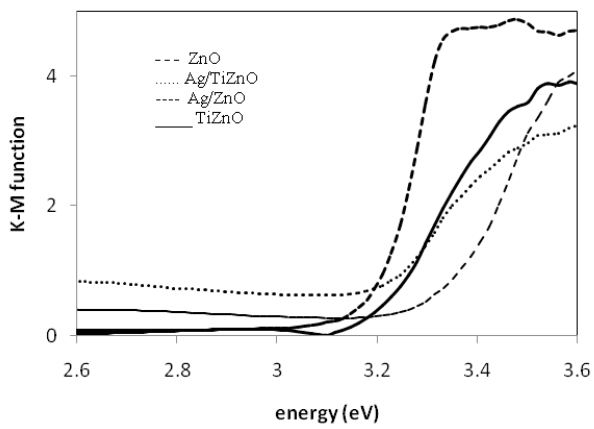


Fig. 5. K–M plots of photocatalysts.

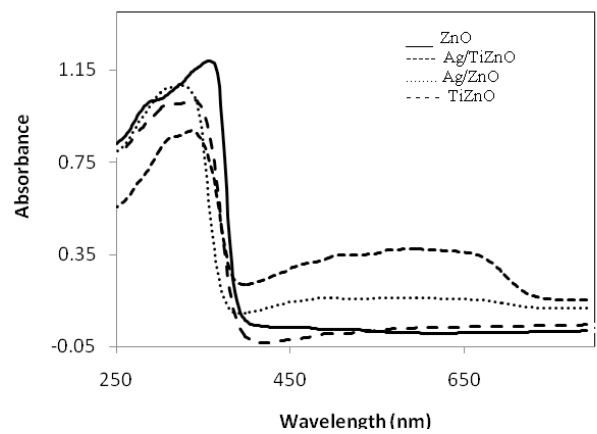


Fig. 6. UV-DRS spectrum of photocatalysts.

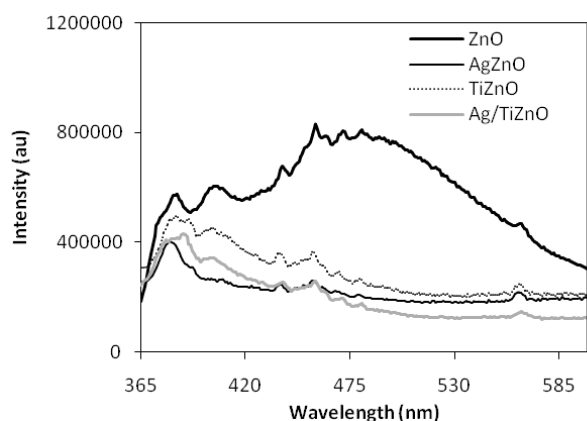


Fig. 7. PL spectra of photocatalysts.

allows the non-irradiative relaxations of excited electrons in ZnO by extracting them into the conduction band (CB) of Ag metal crystallites [7,26,36]. Thus, the Ag metal particles associated with ZnO acts as a sink to store and transport photo-generated electrons, and it is the reason for quenching of PL intensity. Such delocalization of photogenerated electrons within photocatalyst assists to enhance the photocatalytic activity of ZnO [6].

### 3.6. Photocatalytic activity

The photocatalytic activities of the catalysts were compared in terms of the first-order rate constants and half-life period of the reaction (Table 2) under optimized conditions of pH and catalyst dose (supplementary file, Figs. S-5(a–c)).

The results presented in Table 2 reveal that among the four catalysts Ag/TiZnO exhibited the highest photocatalytic activity while Ag/ZnO and TiZnO exhibited higher photocatalytic activity than ZnO. The superior activity of Ag/TiZnO can be accounted in terms of the BET surface area, presence of dopant, i.e., Ti(IV) in it, and coupling of Ag metal particles with TiZnO crystallites. One of the factors governing photocatalytic activities of a catalyst is its surface area. Ti(IV) doping and crystallization of Ag metal in ZnO resulted in the decrease of crystallite size, which reflects into increase in the surface area of the catalyst. Among the four catalysts, ZnO possesses the lowest BET surface area ( $10.3 \text{ m}^2/\text{gm}$ ); therefore, it exhibited the lowest photocatalytic activity. Though the BET, surface areas of three catalysts, i.e., Ag/ZnO ( $16.2 \text{ m}^2/\text{gm}$ ), TiZnO ( $18.6 \text{ m}^2/\text{gm}$ ), and Ag/TiZnO ( $17.1 \text{ m}^2/\text{gm}$ ), are comparable; the catalyst Ag/TiZnO exhibited considerably higher photocatalytic activity. Such high catalytic activity is associated with the delocalization of the excited-state electron from the TiZnO crystal to Ag metal (Fig. 8) [37]. The delocalization of photo-excited electrons decreases the recombination rate of electron-hole pair in base catalyst; therefore, more electron-hole pairs are made available for the chemical reaction at the crystal-liquid interface. Furthermore, Ag metal nanoparticles in the catalyst absorb visible light and form excited Ag atoms, which consist of excited, i.e., hot electrons. These electrons delocalize into CB of base photocatalyst, and thereby, presence of Ag metal increases the activity of the catalyst [26,38].

Table 2  
First-order rate constants and half-life period of the decolourization of the dyes

	OM-2R		ABB		CV	
	$K$ , $\text{min}^{-1}$	$t_{1/2}$ , min	$K$ , $\text{min}^{-1}$	$t_{1/2}$ , min	$K$ , $\text{min}^{-1}$	$t_{1/2}$ , min
ZnO	0.018	37.6	0.025	27.4	0.060	11.6
Ag/ZnO	0.028	25.1	0.060	11.6	0.078	8.9
TiZnO	0.030	23.1	0.076	9.1	0.076	9.1
Ag/TiZnO	0.037	18.8	0.127	5.5	0.099	7.0

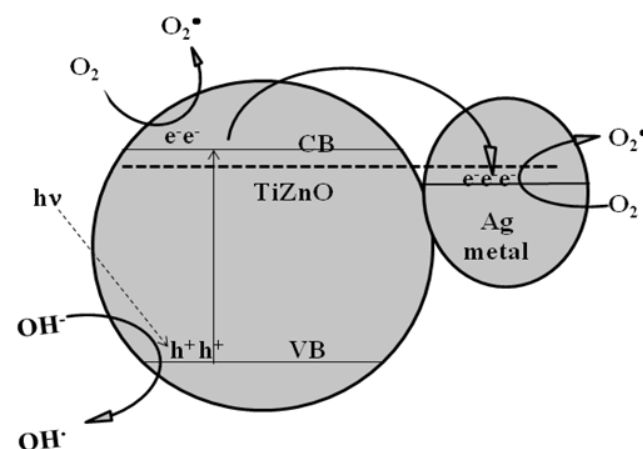


Fig. 8. Sensitization mechanism of ZnO by Ag metal.

The higher activity observed for the Ag/TiZnO over Ag/ZnO can be attributed to the presence of dopant in it and small crystallite sizes TiZnO and Ag metal crystallites in it. Ti(IV) may act as a sink for excited electron and avoid recombination of electron-hole pair. Furthermore, high activity of the Ag/TiZnO over TiZnO can be ascribed to the presence of Ag metal in it [7]. In the Ag/TiZnO photocatalyst, electron-hole pair separation is more efficient due to the presence of both, i.e., dopant and Ag metal, which make it superior catalyst over other presented catalyst in the study.

Electron-hole pairs at the catalyst surface are reaction centres. In alkaline conditions, the hydroxyl-free radical ( $\text{OH}^\cdot$ ) is generated by the trapping of a photo-generated hole by the  $\text{OH}^-$  ion while the oxygen-free radical ( $\text{O}_2^\cdot$ ) is formed by the trapping of a photo-generated electron by dissolved  $\text{O}_2$  in the dye solution (Fig. 7). Both these species are strong oxidizing agents that react with dye molecule and, in a number of steps, result in the mineralization of the dye molecule [2,39].

The different rates of decolourization of the different dyes using the same catalyst can be attributed to the differences in the extent of adsorption of the dyes. Observations showed that dyes adsorbed on the catalyst surface to different extents on account of differences in their structures, charges, and functional groups. It was observed that among the three dyes, CV was most adsorbed dye at the catalyst surface ( $18.73\% \pm 2.56\%$ ) and thereby exhibited the highest decolourization rate; whereas OM-2R was least adsorbed ( $6.44\% \pm 1.84\%$ ) and



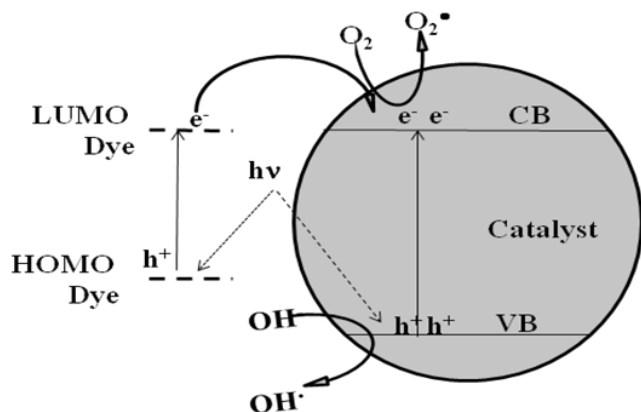


Fig. 9. Sensitization mechanism of ZnO by dye molecules.

exhibited the lowest decolourization rate. The adsorption of dyes results in the surface sensitization of the photocatalyst. ZnO is nearly transparent in visible region while dye molecules exhibit strong absorbance in the same region [38,40]. The dye molecule undergoes electronic excitation with the absorption of sunlight (at or near  $\lambda_{\max}$  of the dye), and the excited-state electron from the dye molecule is injected into the CB of the photocatalyst (Fig. 9). This is the dye sensitized mechanism [33,41]. Such processes extract the electron from the dye and cause the oxidation of the dye molecule as well as supply an electron to the photocatalyst for chemical reaction. Consequently, the adsorption of the dye molecules on the photocatalysts enhances the degradation rate of the dye through the sensitization process [33], and the dye adsorbed to greater extent shows faster rates of decolourization.

### 3.7. Degradation using a channel reactor

From the application viewpoint of photocatalytic degradation of dyes, in the present study, we have performed the degradation of dyes in pilot-scale channel reactor [24]. The performance of the catalyst was evaluated in terms of the decolourization and mineralization of the dyes. Under optimized conditions of pH of dye solution, catalyst dose, and flow rate (of the dye solution), 100% decolourization of all dyes was observed within initial 1–1.5 m length in the reactor. However, it was observed that the just decolourized dye solution had considerably high UV absorbance (Fig. 10) and COD (percent of COD removal at decolourization stage of dye CV = 48.81, ABB = 43.78, and OM-2R = 39.54). Shanthi and Kuzhalosai [42], Yusoff et al. [43], and Singh et al. [44,45] reported similar observations on degradation of different dyes and phenol with ZnO photocatalyst. Decolourization of the dyes at a much faster rate compared with that of mineralization is common because mineralization takes place in stepwise fragmentation of a dye molecule and mineralization is a last step hence it require much longer time [46]. When the decolourized dye solution pass in the forward direction through the reactor, a further decrease in COD and UV absorbance was observed. However, we did not observe 100% removal of UV absorbance and COD of the dye solution, even at a very slow flow rate (2 mL min<sup>-1</sup>) of the dye solutions. The maximum COD removal we observed did not exceed 80% of the original COD for any of the three dye solutions (percent of COD removal CV =

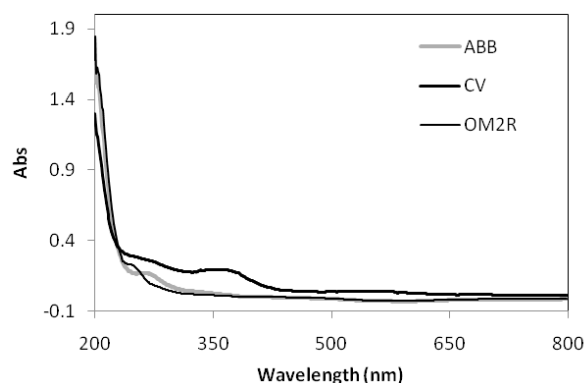


Fig. 10. Absorbance spectra of dyes at decolourization stage in channel reactor.

71.81, ABB = 79.78, and OM-2R = 74.11). This might be due to formation of more stable fragments of the dye molecules that require much more time for degradation and low availability of photocatalyst at end part of the reactor.

## 4. Conclusions

We have successfully synthesized the heterostructured silver metal Ti(IV)-doped ZnO with enhanced photocatalytic activity by facile route. ZnO nanostructures doped with Ti(IV) and consisting of heterostructured silver metal in definite proportion significantly enhanced photocatalytic activity of ZnO. We have demonstrated that channel reactor can be utilized for the removal organic dyes from the aqueous medium by photocatalytic process using sunlight. However, for large-scale application of the reactor, further research work is needed to modify the reactor design so as to attain 100% mineralization and to improve the time required for the completion degradation reaction.

## References

- [1] I.T. Peternel, N. Koprivanac, A.M.L. Bozic, H.M. Kusic, Comparative study of a UV/TiO<sub>2</sub>, UV/ZnO and photo-Fenton processes for the organic reactive dye degradation in aqueous solution, *J. Hazard. Mater.*, 148 (2007) 477–484.
- [2] R.A. Pawar, D.R. Shinde, P.S. Tambade, Synthesis of ZnO photocatalyst via ZnO<sub>2</sub> precursor and its application for dye degradation from effluent under solar irradiation, *Desal. Wat. Treat.*, 57 (2016) 16514–16521.
- [3] S. Chakrabarti, B.K. Dutta, Photocatalytic degradation of model textile dyes in wastewater using ZnO as semiconductor catalyst, *J. Hazard. Mater.*, 112 (2004) 269–278.
- [4] B. Krishnakumar, B. Subash, M. Swaminathan, AgBr–ZnO – an efficient nano-photocatalyst for the mineralization of Acid Black 1 with UV light, *Sep. Purif. Technol.*, 85 (2012) 35–44.
- [5] X. Zhou, G. Liu, J. Yu, W. Fan, Surface plasmon resonance-mediated photocatalysis by noble metal-based composites under visible light, *J. Mater. Chem.*, 22 (2012) 21337–21354.
- [6] M. Thirumavalavan, F.M. Yang, J.F. Lee, Investigation of preparation conditions and photocatalytic efficiency of nano ZnO using different polysaccharides, *Environ. Sci. Pollut. Res.*, 20 (2013) 5654–5664.
- [7] O. Bechambia, M. Chalbi, W. Najjar, S. Sayadi, Photocatalytic activity of ZnO doped with Ag on the degradation of endocrine disrupting under UV irradiation and the investigation of its antibacterial activity, *Appl. Surf. Sci.*, 347 (2015) 414–420.

- [8] S. Kuriakose, V. Choudhary, B. Satpati, S. Mohapatra, Enhanced photocatalytic activity of Ag–ZnO hybrid plasmonic nanostructures prepared by a facile wet chemical method, *Beilstein J. Nanotechnol.*, 5 (2014) 639–650.
- [9] S. Ma, J. Xue, Y. Zhou, Z. Zhang, Photochemical synthesis of ZnO/Ag<sub>2</sub>O heterostructures with enhanced ultraviolet and visible photocatalytic activity, *J. Mater. Chem. A*, 2 (2014) 7272–7280.
- [10] Ö.A. Yıldırım, H.E. Unalan, C. Durucan, Highly efficient room temperature synthesis of silver-doped zinc oxide (ZnO:Ag) nanoparticles: structural, optical, and photocatalytic properties, *J. Am. Ceram. Soc.*, 96 (2013) 766–773.
- [11] Y. Lu, Y. Lin, D. Wang, L. Wang, T. Xie, T. Jiang, Surface charge transfer properties of high-performance Ag-decorated ZnO photocatalysts, *J. Phys. D: Appl. Phys.*, 44 (2011) 315502–315506.
- [12] M.R. Hoffmann, S.T. Martin, W.Y. Choi, D.W. Bahnemann, Environmental applications of semiconductor photocatalysis, *Chem. Rev.*, 95 (1995) 69–96.
- [13] B. Krishnakumar, T. Imae, Chemically modified novel PAMAM-ZnO nanocomposite: synthesis, characterization and photocatalytic activity, *Appl. Catal., A*, 486 (2014) 170–175.
- [14] A. Nezamzadeh-Ejhi, S. Khorsand, Photocatalytic degradation of 4-nitrophenol with ZnO supported nano-clinoptilolite zeolite, *J. Ind. Eng. Chem.*, 20 (2014) 937–946.
- [15] M. Bahrami, A. Nezamzadeh-Ejhi, Effect of the supported ZnO on clinoptilolite nano-particles in the photo-decolorization of semi-real sample bromothymol blue aqueous solution, *Mater. Sci. Semicond. Process.*, 30 (2015) 275–284.
- [16] Q. Deng, X. Duan, D.H.L. Ng, H. Tang, Y. Yang, M. Kong, Z. Wu, W. Cai, G. Wang, Enhanced photocatalytic activity of Ag–ZnO hybrid plasmonic nanostructures prepared by a facile wet chemical method, *ACS Appl. Mater. Interfaces*, 4 (2012) 6030–6037.
- [17] Q. Wang, B. Geng, S. Wang, ZnO/Au hybrid nanoarchitectures: wet-chemical synthesis and structurally enhanced photocatalytic performance, *Environ. Sci. Technol.*, 43 (2009) 8968–8973.
- [18] H. Zeng, P. Liu, W. Cai, S. Yang, X. Xu, Controllable Pt/ZnO porous nanocages with improved photocatalytic activity, *J. Phys. Chem., C*, 112 (2008) 19620–19624.
- [19] L.Q. Jing, D.J. Wang, B.Q. Wang, S.D. Li, B.F. Xin, H.G. Fu, J.Z. Sun, Effects of noble metal modification on surface oxygen composition, charge separation and photocatalytic activity of ZnO nanoparticles, *J. Mol. Catal. A: Chem.*, 244 (2006) 193–200.
- [20] W. Xie, Y. Li, W. Sun, J. Huang, H. Xie, X. Zhao, Surface modification of ZnO with Ag improves its photocatalytic efficiency and photostability, *J. Photochem. Photobiol., A*, 216 (2010) 149–155.
- [21] Y. Zheng, L. Zheng, Y. Zhan, X. Lin, Q. Zheng, K. Wei, Y. Zheng, L. Zheng, Y. Zhan, X. Lin, Q. Zheng, K. Wei, Ag/ZnO heterostructure nanocrystals: synthesis, characterization, and photocatalysis, *Inorg. Chem.*, 46 (2007) 6980–6986.
- [22] X. Cao, X. Lan, Y. Guo, Z. Cui, S. Han, J. Wang, Q. Zhao, Preparation and characterization of bifunctional ZnO/ZnS nanoribbons decorated by  $\gamma$ -Fe<sub>2</sub>O<sub>3</sub> clusters, *J. Phys. Chem., C*, 111 (2007) 18958–18964.
- [23] H.B. Fu, T.G. Xu, S.B. Zhu, Y.F. Zhu, Photocorrosion inhibition and enhancement of photocatalytic activity for ZnO via hybridization with C-60, *Environ. Sci. Technol.*, 42 (2008) 8064–8069.
- [24] R. Ostermann, D. Li, Y. Yin, J.T. McCann, Y. Xia, V<sub>2</sub>O<sub>5</sub> nanorods on TiO<sub>2</sub> nanofibers: a new class of hierarchical nanostructures enabled by electrospinning and calcination, *Nano Lett.*, 6 (2006) 1297–1302.
- [25] C. Abed, C. Bouzidi, H. Elhouichet, B. Gelloz, M. Ferid, Mg doping induced high structural quality of sol–gel ZnO nanocrystals: application in photocatalysis, *Appl. Surf. Sci.*, 349 (2015) 855–863.
- [26] Y.I. Choia, H.J. Jung, W.G. Shin, Y. Sohn, Band gap-engineered ZnO and Ag/ZnO by ball-milling method and their photocatalytic and Fenton-like photocatalytic activities, *Appl. Surf. Sci.*, 356 (2015) 615–625.
- [27] L. Shen, N. Bao, K. Yanagisawa, K. Domen, A. Gupta, C.A. Grimes, Direct synthesis of ZnO nanoparticles by a solution-free mechanochemical reaction, *Nanotechnology*, 17 (2006) 5117–5123.
- [28] A.I. Vogel, *Quantitative Inorganic Analysis, Including Elementary Instrumental Analysis*, 3rd ed., ELBS, London, 1963, pp. 354, 654.
- [29] D.R. Shinde, I. Qureshi, R.A. Pawar, R.R. Pawar, Enhancement of photocatalytic activity of ZnO via Nd(III) doping towards the degradation of dyes under solar irradiation, *J. Nanoeng. Nanomanuf.*, 5 (2015) 197–203.
- [30] D.R. Shinde, R.A. Pawar, Zinc oxide mediated photocatalytic degradation of azo dye Amido Black B-10 in channel reactor under solar irradiation, *J. Nanoeng. Nanomanuf.*, 5 (2015) 192–196.
- [31] S. Kanade, Synthesis, Characterization of ZnO and Ag Metal/Ti(IV) doped ZnO and Their Application for Degradation of Dyes under Solar Irradiation, MPhil Thesis (Savitribai Phule Pune University, Pune, India), 2015, pp. 57–59.
- [32] R. Georgekutty, M.K. Seery, S.C. Pillai, Effect of silver modification on the photocatalytic activity of nanocrystalline ZnO, *J. Phys. Chem., C*, 112 (2008) 13563–13570.
- [33] B. Subash, B. Krishnakumar, M. Swaminathan, M. Shanthi, Highly efficient, solar active, and reusable photocatalyst: Zr-loaded Ag–ZnO for Reactive Red 120 dye degradation with synergistic effect and dye sensitized mechanism, *Langmuir*, 29 (2013) 939–949.
- [34] L. Duan, B. Lin, W. Zhang, S. Zhong, Enhancement of ultraviolet emissions from ZnO films by Ag doping, *Appl. Phys. Lett.*, 88 (2006) 232110–232115.
- [35] B.J. Niu, L.L. Wu, W. Tang, X.T. Zhang, Q.G. Meng, Enhancement of near-band edge emission of Au/ZnO composite nanobelts by surface plasmon resonance, *CrystEngComm*, 13 (2011) 3678–3681.
- [36] Y. Liang, N. Guo, L. Li, R. Li, G. Ji, S. Gan, Fabrication of porous 3D flower-like Ag/ZnO heterostructure composites with enhanced photocatalytic performance, *Appl. Surf. Sci.*, 332 (2015) 32–39.
- [37] L. Xu, B. Wei, W. Liu, H. Zhang, C. Su, J. Che, Flower-like ZnO-Ag<sub>2</sub>O composites: precipitation synthesis and photocatalytic activity, *Nanoscale Res. Lett.*, 8 (2013) 536–541.
- [38] Y. Zang, J. Yin, X. He, C. Yue, Z. Wu, J. Li, J. Kang, Plasmonic-enhanced self-cleaning activity on asymmetric Ag/ZnO surface-enhanced Raman scattering substrates under UV and visible light irradiation, *J. Mater. Chem., A*, 2 (2014) 7747–7753.
- [39] A.B. Patil, K.R. Patil, S.K. Pardeshi, Ecofriendly synthesis and solar photocatalytic activity of S-doped ZnO, *J. Hazard. Mater.*, 183 (2010) 315–323.
- [40] L. Qi, J. Yu, G. Liu, P.K. Wong, Synthesis and photocatalytic activity of plasmonic Ag@AgCl composite immobilized on titanate nanowire films, *Catal. Today*, 224 (2014) 193–199.
- [41] P. Muthirulan, M. Meenakshisundaram, N. Kannan, Beneficial role of ZnO photocatalyst supported with porous activated carbon for the mineralization of alizarin cyanin green dye in aqueous solution, *J. Adv. Res.*, 4 (2013) 479–484.
- [42] M. Shanthi, V. Kuzhalosai, Photocatalytic degradation of an azo dye, Acid Red 27, in aqueous solution using nano ZnO, *Indian J. Chem.*, 51 (2012) 428–434.
- [43] N. Yusoff, L.N. Ho, S. Ong, Y. Wong, W.F. Khalik, Photocatalytic activity of zinc oxide (ZnO) synthesized through different methods, *Desal. Wat. Treat.*, 57 (2016) 12496–12507.
- [44] N.K. Singh, S. Saha, A. Pal, Methyl red degradation under UV illumination and catalytic action of commercial ZnO: a parametric study, *Desal. Wat. Treat.*, 56 (2015) 1066–1076.
- [45] N.K. Singh, S. Saha, A. Pal, Solar light-induced photocatalytic degradation of methyl red in an aqueous suspension of commercial ZnO: a green approach, *Desal. Wat. Treat.*, 53 (2015) 501–514.
- [46] S. Saha, J.M. Wang, A. Pal, Nano silver impregnation on commercial TiO<sub>2</sub> and a comparative photocatalytic account to degrade malachite green, *Sep. Purif. Technol.*, 89 (2012) 35–44.



## Supplementary data

Table S-1  
Structure of dye and  $\lambda_{\max}$  of dyes

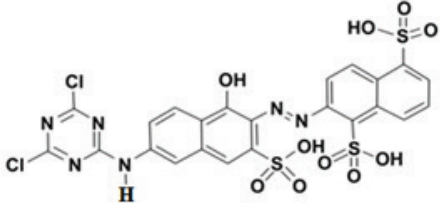
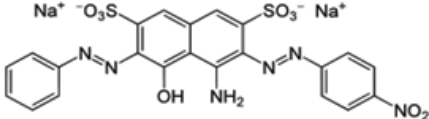
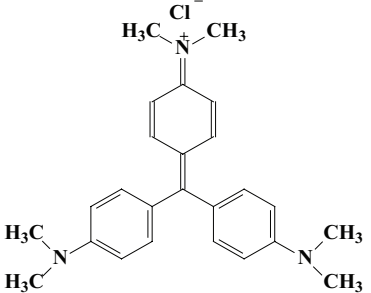
Sr. No.	Name of the dye	Structure	$\lambda_{\max}$ and pH of dye solution	Molecular weight
1	Orange M2R (OM-2R)	 <p>Molecular formula: <math>C_{23}N_3H_{16}Cl_2N_6S_3O_{10}</math></p>	498.8 nm, pH = 7	712.47 g
2	Amido Black B-10 (ABB)	 <p>Molecular formula: <math>C_{22}H_{14}N_6Na_2O_9S_2</math></p>	620.6 nm, pH = 7	616.49 g
3	Crystal violet (CV)	 <p>Molecular formula: <math>C_{25}H_{30}ClN_3 \cdot 9H_2O</math></p>	592.4 nm, pH = 7	269.31 g

Table S-2  
Effect of catalyst dose on the dye degradation

Weight of ZnO per litre, mg	% Degradation for ABB	% Degradation for OM-2R	% Degradation for CV
100	47.24 ± 0.98	50.52 ± 0.83	56.87 ± 0.74
200	58.92 ± 1.24	63.14 ± 1.56	71.28 ± 1.01
300	78.06 ± 0.50	76.76 ± 1.05	89.06 ± 0.69
400	87.35 ± 1.33	90.10 ± 1.11	92.63 ± 0.86
500	87.24 ± 1.16	89.15 ± 1.03	93.14 ± 0.88

Table S-3  
Comparison of photocatalytic activity of catalysts in terms of % degradation

Catalyst	% Degradation for ABB	% Degradation for OM-2R	% Degradation for CV
Ag (0%)/Ti <sub>0.10</sub> Zn <sub>0.9</sub> O	39.81 ± 1.13	28.43 ± 1.15	34.5 ± 1.05
Ag (3.5%)/Ti <sub>0.075</sub> Zn <sub>0.9</sub> O	46.33 ± 0.93	31.90 ± 1.55	36.13 ± 0.85
Ag (7%)/Ti <sub>0.05</sub> Zn <sub>0.9</sub> O	90.54 ± 1.40	83.57 ± 0.94	89.73 ± 0.91
Ag (10.5%)/Ti <sub>0.025</sub> Zn <sub>0.9</sub> O	71.46 ± 1.40	70.97 ± 1.06	77.70 ± 0.50
Ag (14%)/Ti <sub>0.0</sub> Zn <sub>0.9</sub> O	55.37 ± 1.55	62.34 ± 0.99	57.47 ± 0.80
Pure ZnO	61.38 ± 1.93	63.50 ± 0.68	68.47 ± 1.27

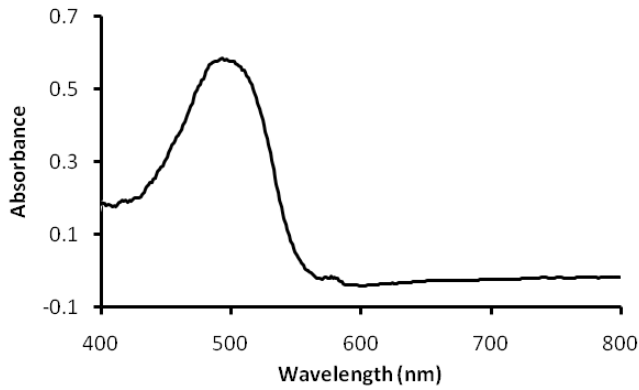


Fig. S-1(a). Absorption spectra of OM-2R dye.

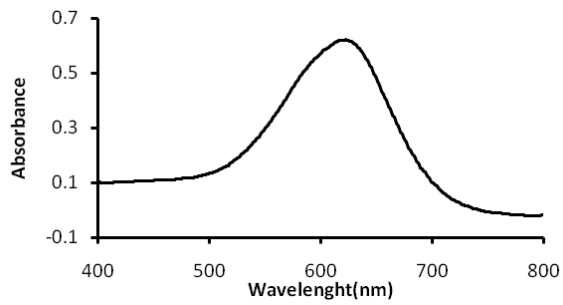


Fig. S-1(b). Absorption spectra of ABB dye.

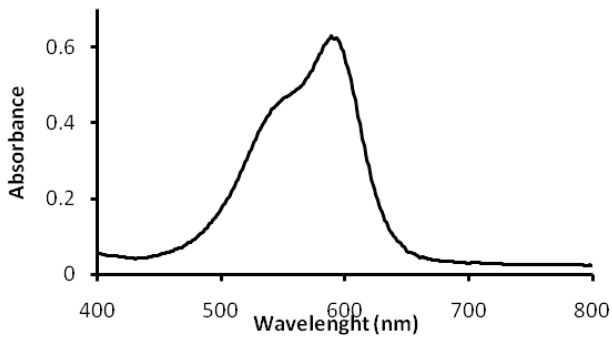


Fig. S-1(c). Absorption spectra of CV dye.

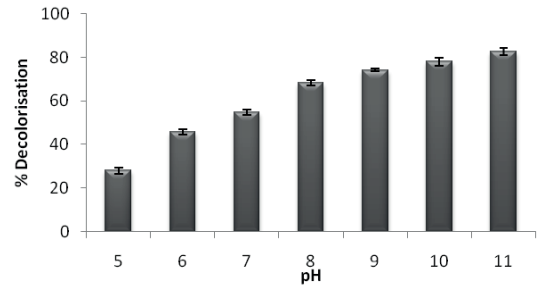


Fig. S-2(a). Influence of pH on % degradation of OM-2R.

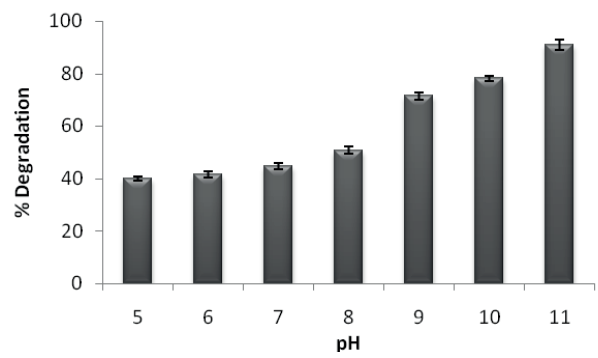


Fig. S-2(b). Effect of pH on % degradation of ABB.

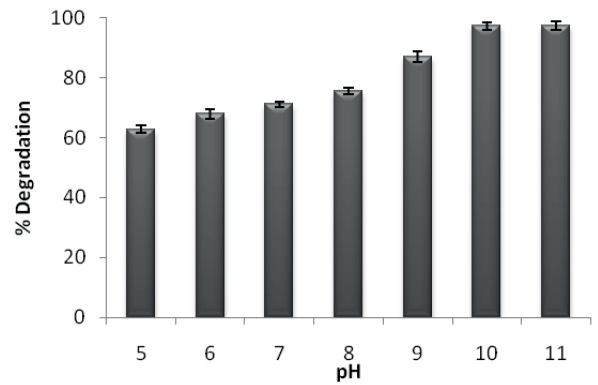


Fig. S-2(c). Influence of pH on degradation of CV.

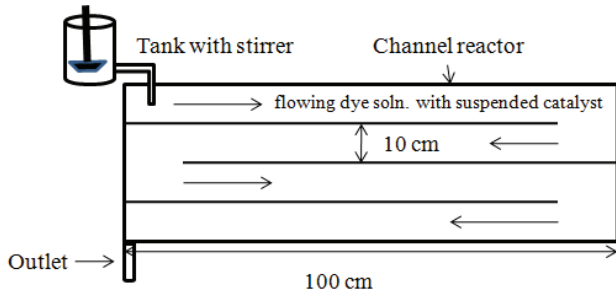


Fig. S-3. Design of channel reactor.

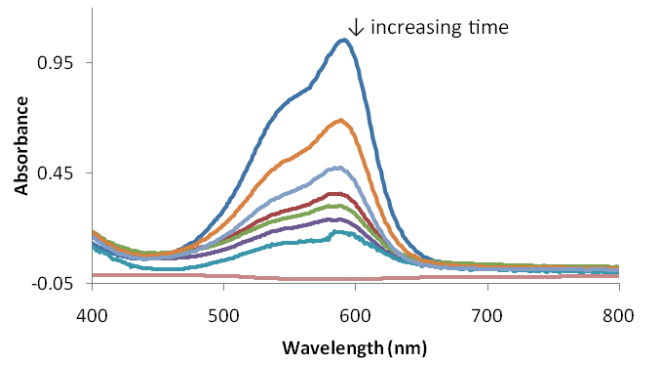


Fig. S-5(a). Absorbance spectra of CV at different time interval in kinetics of decolourization.

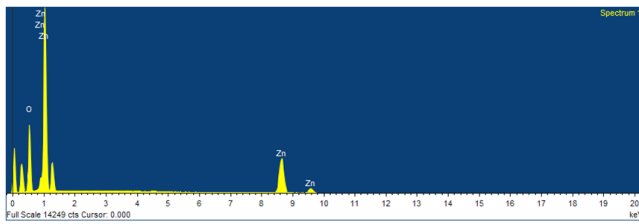


Fig. S-4(a). EDS of ZnO.

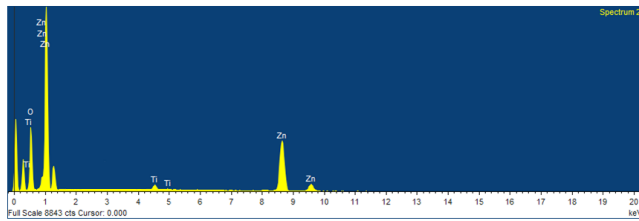


Fig. S-4(b). EDS of TiZnO.

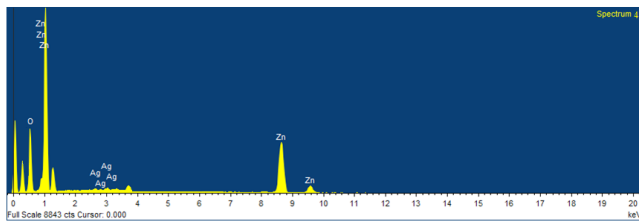


Fig. S-4(c). EDS of heterostructured Ag metal/ZnO.

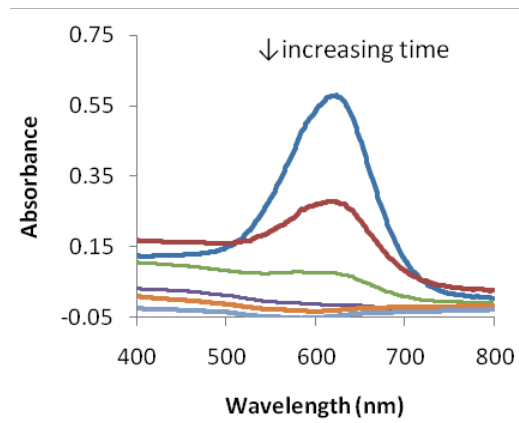


Fig. S-5(b). Absorbance spectra of ABB at different time interval in kinetics of decolourization.

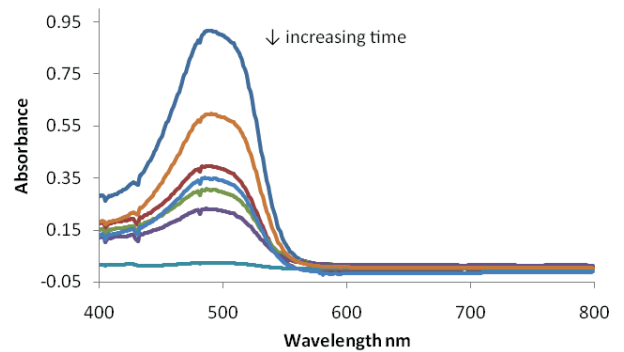


Fig. S-5(c). UV-visible spectra of OM-2R at different time interval of kinetic of decolourization.